Ultramicroscopy 109 (2009) 247–252

Contents lists available at ScienceDirect

Ultramicroscopy

journal homepage: www.elsevier.com/locate/ultramic

Nanotribological properties of precision-controlled regular nanotexture on H-passivated Si surface by current-induced local anodic oxidation

Yufei Mo [a,b], Wenjie Zhao [a,b], Deming Huang [a,b], Fei Zhao [a,b], Mingwu Bai [a,*]

[a] State Key Laboratory of Solid Lubrication, Lanzhou Institute of Chemical Physics, Chinese Academy of Sciences, Lanzhou 730000, PR China
[b] Graduate School of Chinese Academy of Sciences, Beijing 100039, PR China

ARTICLE INFO

Article history:
Received 22 July 2008
Received in revised form
19 October 2008
Accepted 29 October 2008

Keywords:
Nanotexture
Local anodic oxidation
Atomic force microscopy
Nanotribology

ABSTRACT

Nano-sized textures resulted from localized electrochemical oxidation by using atomic force microscopy (AFM) were fabricated on H-passivated Si surface. In this paper, the fabrication and nanotribological properties of nanotexture by local anodic oxidation (LAO) on H-passivated Si surface are presented. A special attention is paid to find the relation between the size of oxide nanotexture and operational parameters such as tip-sample pulsed bias voltage, pulsewidth, and relative humidity to fabricate oxide nanotexture. The nanotribological properties were investigated by a colloidal probe. The results indicate that the nanotextures exhibited low adhesion and greatly reduced friction force at nanometer scale.

1. Introduction

Over the last decade, nanotechnologies have become one of the promising research areas which might bring a significant process into material and device development [1]. At present, there is a wide spectrum of technological approaches capable of producing nanostructures; however, none of them can be considered as an ideal and generally acceptable tool [2]. Local anodic oxidation (LAO) performed by atomic force microscopy (AFM) is an attractive technique to fabricate nanometer scale oxide regions on the surface for device patterning [3,4]. The LAO process can be used in not only fabrication of nanodevices but also adhesion-resistance and friction-reduction as surface texture. Fabrication and application of nanotextures for a study of their unique quantum properties and for building various nano patterns require a reliable control of individual technological step. To prepare nanostructures of required dimension and property, the relations among the operation parameters of the fabrication should be fairly understood. In previous studies, AFM LAO has been demonstrated as the most promising tool for fabricating nanodots and lines on several types of materials ranging from metals and semiconductors [5–13]. However, the outermost part of metal and silicon converts to their oxide under ambient conditions, which might reduce lateral resolution of nanotextures. Furthermore, so far their mechanical properties have not been reported as far as we know.

Silicon has been widely used as micromechanical material. High thermal conductivity, large break down field, and high saturation velocity makes it as an ideal choice for high temperature, high power, and high voltage electronic devices. In addition, its physicochemical stability, high melting temperature, extreme hardness make silicon as an attractive material for fabricating sensors and actuators that are capable of performing in harsh environments, such as high temperature, and corrosive and abrasive media. However, from a tribological point of view, adhesion-resistance and friction-reduction of this material can be further improved [14]. The H-passivated Si substrate is hydrogen passivated by leaking H_2 into an ultrahigh vacuum (UHV) chamber, where atomic H was created by creaking H_2 molecules on a hot tungsten filament. The process can prevent silicon converting to a nonuniform native oxide [15]. In order to improve the resolution of oxide nanotexture and investigate their nanotribological properties, we focus on the fabrication of nanotextures on H-passivated Si substrate by LAO.

AFM has been used extensively to measure adhesive forces and friction between surfaces in nanoscale. Nanoadhesive forces come from two sources: contact interfacial forces and noncontact forces such as Van Der Waals or electrostatic forces. Adhesion is typically measured by a pull-off force between the cantilever tip and the surface. The challenge in the measurement often lies with the determination of real area of contact. For sharp tips, the surface roughness and high contact pressure may cause the tip to rotate and the surface to deform. Ducker [16] introduced the use of colloidal probe tips by attaching a sphere to the cantilever to measure adhesion. The spherical shape of the tip provides controlled contact pressure, symmetry, and mostly elastic

* Corresponding author. Tel.: +86 931 4968080; fax: +86 931 4968163.
E-mail address: mwbai@LZB.ac.cn (M. Bai).

0304-3991/$ - see front matter © 2008 Published by Elsevier B.V.
doi:10.1016/j.ultramic.2008.10.025

contacts. To LAO nanotexture adhesion measurement, the spherical probe tip can fully contact with texture surface, while sharp tip can only point contact. However, the measurement of the contact surface roughness of a colloidal probe poses additional challenges. Since the total surface area are very small, therefore, we adopted the reverse AFM imaging method developed by Neto [17] to identify the contact location and directly imaged by an AFM with a sharp tip to provide detailed three-dimensional surface topography.

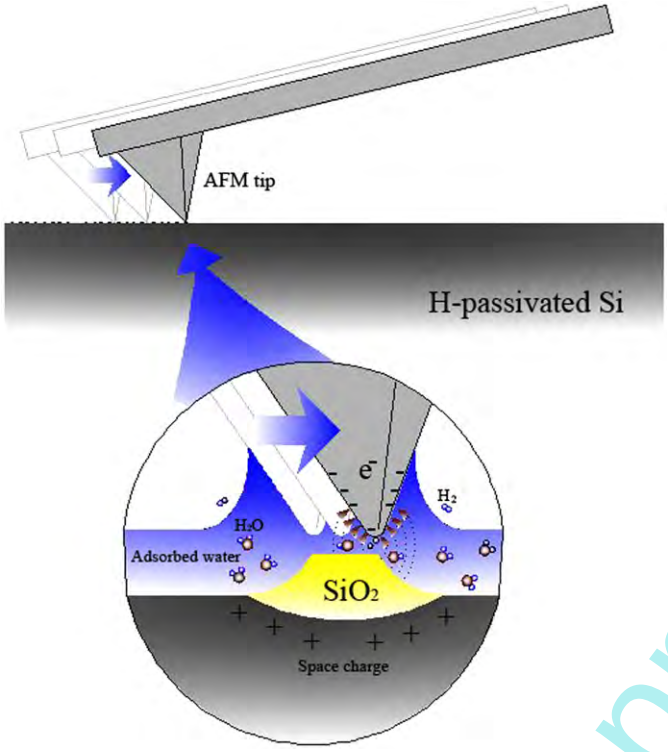

Fig. 1. Schematic of the local anodic-oxidation process induced by a biased conductive AFM tip.

2. Experimental

Fabrication of nanotextures was performed by using a commercial AFM (CSPM 4000). The LAO was carried out in the contact mode and in the regime of the contact force using silicon cantilevers with electrically conductive tips coated by platinum (Budget sensor). The tip is conic and the radius is below 25 nm. The AFM software was extended with a program package for the well-defined movement of the tip over a sample. The facility associated with control of other tip-sample parameters gave us possibility to accomplish pre-defined patterns at various pulsed bias voltage, pulsewidth and write speed in contact mode. For environmental control, relative humidity was controlled by introducing a mixture of dry and moist nitrogen stream inside the booth, while the temperature was maintained at $10\pm1\,^{\circ}C$. The relative humidity was controlled to range from 15% to 80%. In this nanolithography process, oxides grow on a chemically reactive substrate by the application of a pulse bias voltage between a conductive tip and a sample surface which acts as an anode. The LAO process performed by AFM is illustrated in Fig. 1. The driving force is the faradaic current flows between the tip and sample surface with the aid of the water meniscus. When the faradaic current flows into water bridge, H_2O molecules are decomposed into oxyanions (OH^-, O^-) and protons (H^+). These ions penetrate into the oxide layer due to a high electric field ($E>10^7\,V/m$) [18], leading to the formation and subsequent growth of SiO_2 on the Si surface.

For adhesion measurement of the fabricated nanotextures, colloidal probe was prepared by gluing glass sphere with a radius of 40 μm onto the individual tipless cantilever. The cantilever used in our experiments was etched from single-crystal silicon, and the force constant of the cantilever was calculated using the individually measured thickness, width and length [19]. The above dimensions were determined by a scanning electron microscope,

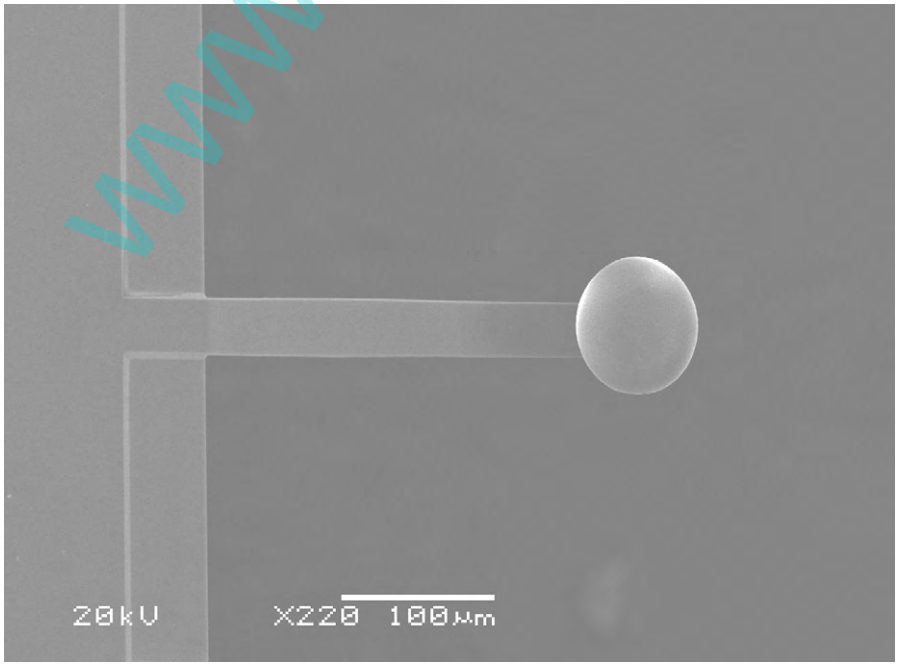

Fig. 2. SEM image of the colloidal probe.

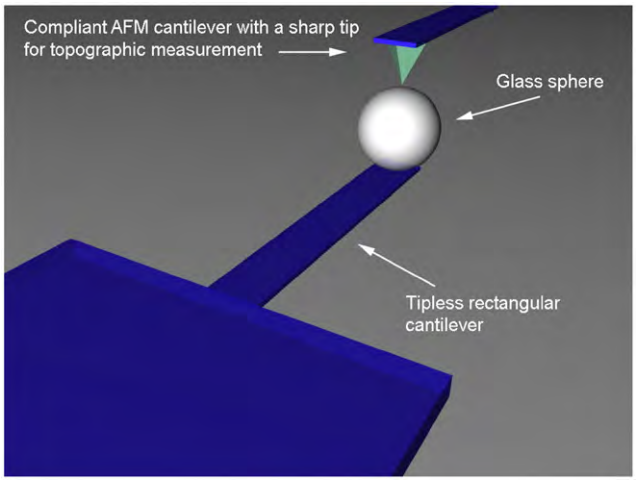

Fig. 3. A schematic illustration on topographic measurment of colloidal probe.

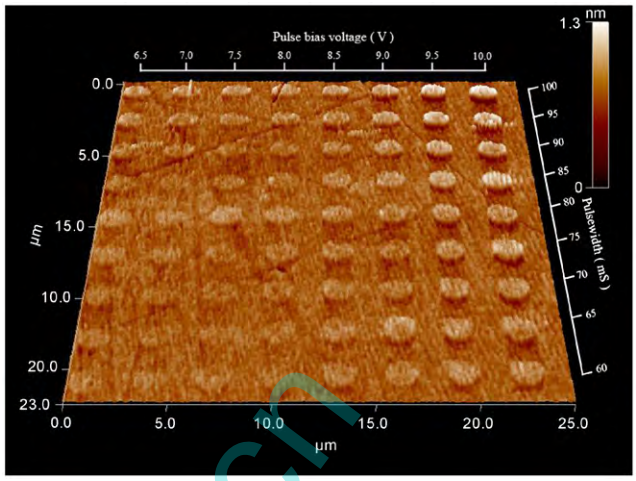

Fig. 4. A testing array of Si pillars prepared at different tip-sample voltages and pulsewidths on a Si substrate (relative humidity of 15% RH, temperature of 10 °C).

and the normal force constant of the cantilever was determined to be 0.275 N/m, which is close to the announced force constant 0.30 N/m. A typical colloidal probe is shown in Fig. 2. The colloidal probe was cleaned by ethanol and acetone in turn before use. For all measurements the same cantilever was used in this comparative study. Furthermore, to avoid the influence of molecules which may transfer to the tip on the AFM/FFM experiments, the tip was scanned on a cleaved mica surface to remove these physically adsorbed molecules. The surface topography of the colloidal probe was scanned with a force constant of 0.12 N/m cantilever and a silicon nitride sharp tip under contact mode, as shown in Fig. 3. The relative humidity was controlled at 15% RH. Repeated measurements were within 5% of the average value for each sample.

The friction force is a lateral force exerted on a colloidal probe during scanning and can be measured using the twist of the cantilever. To obtain friction data, the spherical tip was scanned back and forth in the *x*-direction in contact with the sample at a constant load, while the lateral deflection of the lever was measured. The differences in the lateral deflection or friction signal between back and forth motions are proportional to the friction force. The friction force was calibrated by the method described in Ref. [20]. Friction forces were continuously measured with various external loads. The load was increased linearly in each successive scan line and normal loads ranged from 10 to 150 nN.

3. Results and discussion

3.1. Fabrication of local anodic-oxidation nanotextures

The LAO process is controlled by several major parameters as follows: pulsed bias voltage, pulsewidth and humidity. Fig. 4 shows a testing array of Si oxide pillars that was prepared at different tip-sample voltages and pulsewidths on H-passivated Si substrate (relative humidity of 15%, temperature of 10 °C). From top to bottom in this figure, the pillars were prepared at progressively lower tip-sample pulse bias voltages. On the other hand, going from right to left, the pillars were made at progressively decreasing pulsewidths. It is obvious that the pillar was prepared at the highest tip-sample pulse voltage and the longest pulsewidth is best developed one in height. Such a testing pillar array makes it possible to find the relation between the height of pattern and operational parameters.

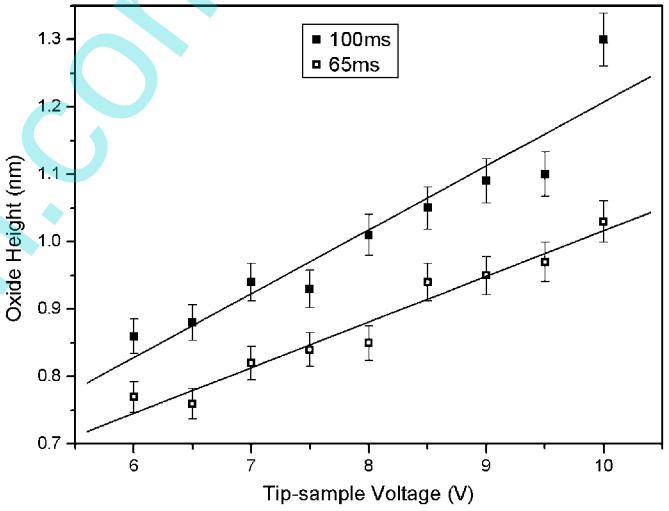

Fig. 5. The oxide height as a function of tip-sample pulse bias voltage for two distinct pulsewidths at relative humidity of 15%.

Fig. 5 shows the oxide height as a function of tip-sample pulse bias voltage for two distinct pulsewidths at a relative humidity of 15%. The height of Si oxide pillars showed a linear dependence on tip-sample pulse bias voltage. From the experiment, the lowest value (0.76 nm) of pillar was approached at a pulse bias voltage of 6 V and pulsewidth of 65 ms. On the other hand, the highest value (1.3 nm) of the pillar was achieved at a pulse bias voltage of 10 V and pulsewidth of 100 ms. Fig. 6 shows the oxide height as a function of pulsewidth for various tip-sample pulse bias voltages at relative humidity of 15%. As shown in the figure, the height of Si oxide pillars exhibited a linear increase with pulsewidth. In the case of patterning oxide pillars, the effectiveness of the tip-sample pulse bias voltages suggested that the fabrication of pillars can be achieved by varying the pulsewidth. It is evident that the lower pulse bias voltages and short pulsewidths result in lower anodized oxide pillars. The reason for that could be due to no enough voltage or time for reaching the saturation height. In anodic-oxidation process, the anionic and cationic transport is an important factor in determining the kinetics of oxidation. In test condition, the driving force is the faradic current flowing between the tip and sample surface, with aid of the water meniscus. Compared to the previous study [21–23], the H-passivated Si can

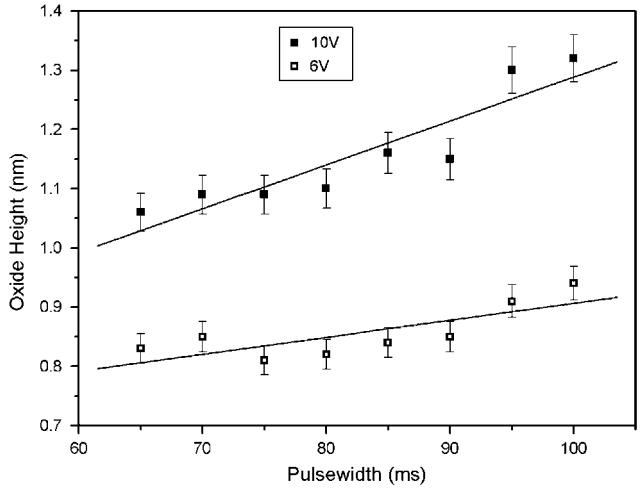

Fig. 6. The oxide height as a function of pulsewidth for various tip-sample pulse bias voltages at relative humidity of 15%.

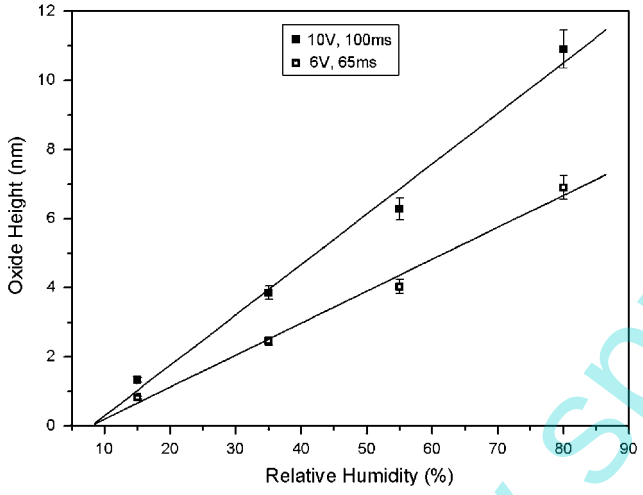

Fig. 7. The height of Si oxide as a function of relative humidity, for two distinct optional parameters (pulse bias voltage and pulsewidth).

have higher growth rate and larger saturated oxide height than that of common p- or n-type Si under similar oxidation conditions. Fig. 7 demonstrates the linear dependences of the oxide height as a function of relative humidity. The height of Si oxide pillars was proportional to the relative humidity for two distinct optional parameters (pulse bias voltage and pulsewidth). The highest value (11 nm) of pillar was achieved at a pulse bias voltage of 10 V, pulsewidth of 100 ms and relative humidity of 85%. This value is much higher than the highest value (1.3 nm) of pillar under relative humidity of 15%, with same pulse bias voltage and pulsewidth. The reason for the result could be due to the difference in the thickness of the water film on the H-passivated Si surface under different relative humidity. In any case, the present results demonstrate that the AFM current-induced local oxidation can be a viable tool for fabricating well-controlled oxide nanotextures, provided proper operation conditions are chosen.

3.2. Nanotribological properties of nanotextures

Adhesion is generally measured by the amount of force necessary to separate two surfaces in contact. At nanoscale, mechanical loading is often not the overwhelming force as in macroscale, and surface forces such as Van Der Waals, electronic,

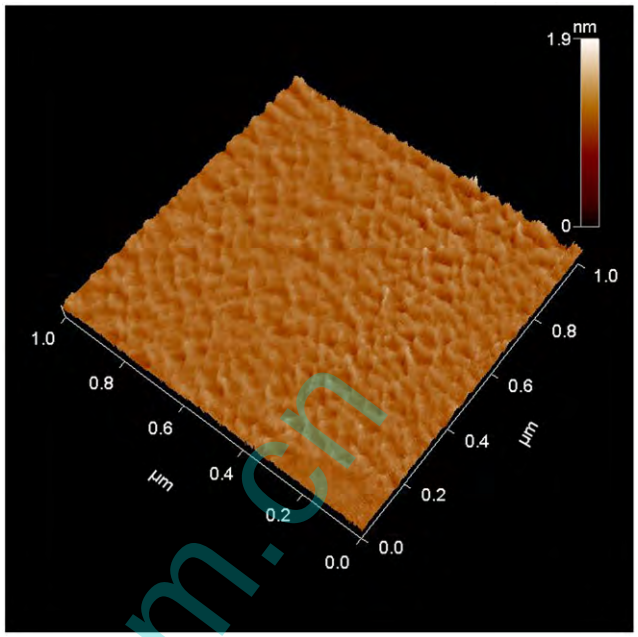

Fig. 8. AFM topography of the colloidal probe tip surface.

and capillary/meniscus forces become significant in controlling the pull-off force. Fig. 8 shows the three-dimensional surface topography of a colloidal probe. The microroughness of the colloidal probe in root-mean-square (RMS) of the monolayer was estimated to be 0.1 nm over an area of $1 \times 1\,\mu m^2$ (512×512 resolution). Fig. 9a–c show surface coverage of nano pillars of 3%, 8% and 12% were fabricated by LAO at a pulse bias voltage of 10 V, pulsewidth of 100 ms and relative humidity of 85%. The height of pillars was measured as about 11 nm by AFM, therefore, the nanotextures tend to dominate the contact condition as compared to the colloidal probe. It is observed that the adhesive forces are closely related to the surface coverage of nanotextures, as shown in Fig. 10. Strong adhesion is observed on bare H-passivated Si surface, on which the adhesive force is as high as about 175 nN. Once the surface coverage of nanotextures of 12%, 8%, and 3% were fabricated on H-passivated Si surface, the adhesive force were greatly decreased to 105, 70, and 52 nN, respectively. This result indicates that the nanotextures have good adhesion-resistance on H-passivated Si surface. The surface coverage relates directly to the bearing ratio, which describes the real area of contact between two solid surfaces [24]. Holding the height of nano pillars the same, the higher the surface coverage, the higher the bearing ratio. Therefore, the adhesive force decreases as density of nano pillars decreases, or as the distance between the nano pillars increase, because low density means fewer contacting points. Larger meniscus area results in higher adhesion. As surface coverage of the nano pillars increases, not only can each meniscus grow bigger, the capillary pressure with each meniscus also became higher [25]. Both of these changes lead to higher adhesive force.

Fig. 11 presents that the friction forces are closely related to the surface coverage of the nano pillar. Nanotextures evidently reduced the friction force, and especially the surface coverage of nano pillar of 3% exhibited lowest friction force, while H-passivated Si showed strong friction force. Above observations could be explained by taking into account the adhesion between the tip and the surface. Considering the adhesion, F_f (F_n) behavior can be described in a general form [26]

$$F_f = C_1 F_n^m + C_2 F_n + C_3$$

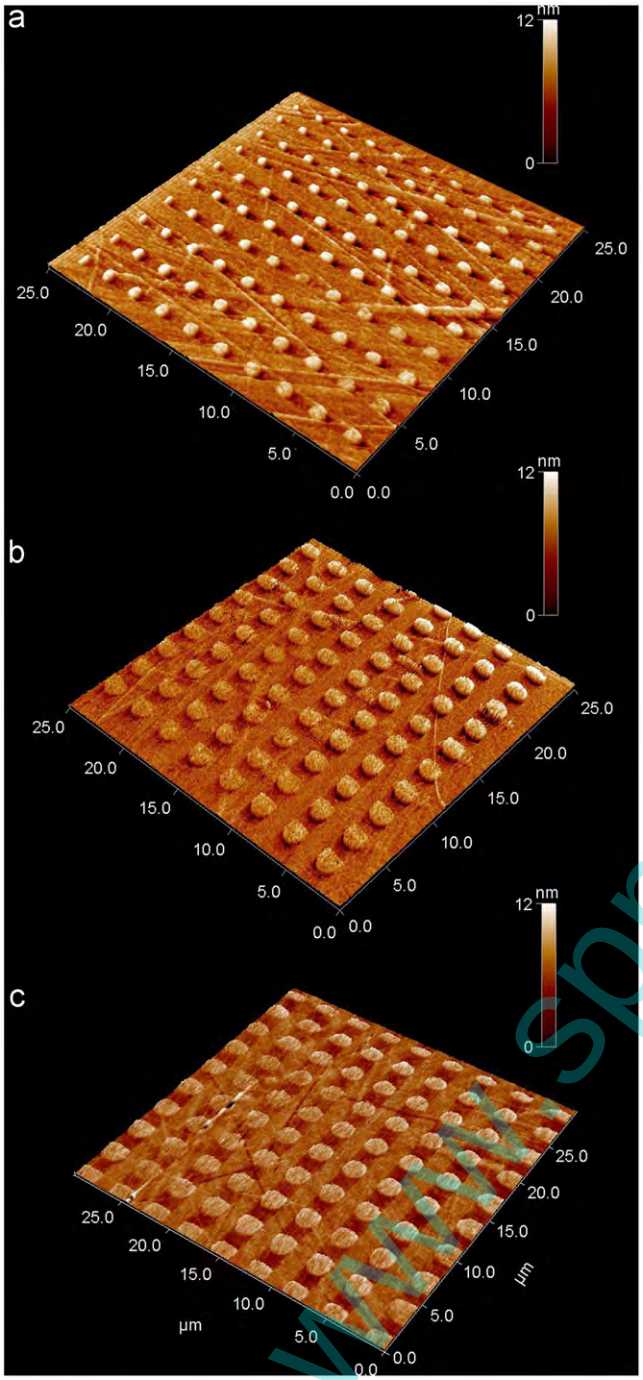

Fig. 9. AFM topographies of various surface coverage of nanotextures of (a) 3%, (b) 8%, and (c) 12%.

where F_f and F_n are the friction force and the external load, respectively. C_1, C_2, and C_3 are material-dependent constants, and the index m ($0<m<1$) depends on the asperity shape ($m = 2/3$ for sphere/plane contact). The first term in the equation is closely related to the adhesion of interacting surfaces, and the second term is referred to shear fraction of friction. For contacts of solid surfaces without adhesive agents, adhesion is proportional to the real area of contact, which results in less adhesive energy dissipation during sliding on nanotextures surface. In addition, the surface nanotextures between the sliding pair act as a shock absorber to reduce the amount of impact energy transferred to the substrate, which may allow for friction-reduction under higher frequent reciprocating movement.

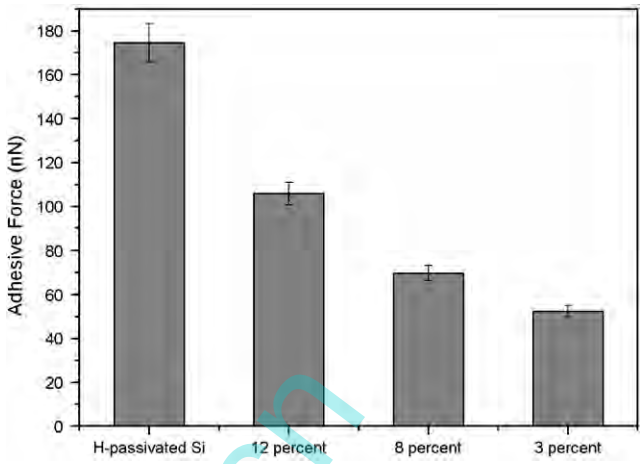

Fig. 10. Adhesive forces between AFM colloidal probe and surfaces of bare H-passivated Si and nanotextures with surface coverage of 12%, 8%, and 3%, at relative humidity of 15%.

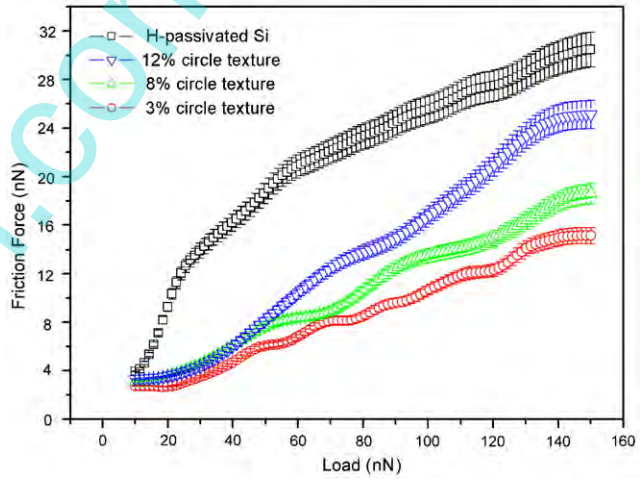

Fig. 11. Plots of friction and load for surface of H-passivated Si and nanotextures with surface coverage of 12%, 8%, and 3% at a scanning velocity of 25 μm/s (15% RH).

4. Summary and conclusions

In the paper, the application of current-induced LAO for the fabrication of nanotextures on H-passivated Si surface is presented. The results indicate that the height of the nanotextures could be precision controlled by several major operational parameters as tip-sample pulse bias voltage, pulsewidth and relative humidity. The H-passivated Si shows higher growth rate and larger oxide height than that of common p- or n-type Si under similar oxidation conditions. The various surface coverage of nano pillar was fabricated for the purpose of adhesion-resistance and friction-reduction. In the current study, strong adhesion is observed on bare H-passivated Si surface, on which the adhesive force is as high as about 175 nN. Once the surface coverage of nanotextures of 12%, 8%, and 3% were fabricated on H-passivated Si surface, the adhesive force were greatly decreased to 105, 70, and 52 nN, respectively. In addition, surface nanotextures evidently reduced the friction force, and especially the surface coverage of nano pillar of 3% exhibited lowest friction force. The H-passivated Si treated with nanotexture exhibits better adhesion-resistance and friction-reduction than untreated Si in

nanoscale. Thus, we believe this technique to be potentially applicable to the fabrication of surface modification and nanodevices.

Acknowledgment

This work was funded by the National Natural Science Foundation of China under Grant no. 50675217 and National 973 Program: 2007CB607601.

References

[1] G. Timp, Nanotechnology, Springer, New York, 1999.
[2] Nanotech, Scientific American September 2001 (special issue).
[3] J.A. Dagata, Science 270 (1995) 1625.
[4] Y.F. Mo, Y. Wang, M.W. Bai, Physica E 41 (2008) 146.
[5] Z. Chen, S. Hou, H. Sun, X. Zhao, J. Phys. D: Appl. Phys. 37 (2004) 1357.
[6] P. Avouris, T. Hertel, R. Martel, Appl. Phys. Lett. 71 (1997) 285.
[7] M. Yang, Z. Zheng, Y. Liu, B. Zhang, Nanotechnology 17 (2006) 330.
[8] Y. Okada, S. Amano, M. Kawabe, J.S. Harris, J. Appl. Phys. 83 (1998) 7998.
[9] S.R. Jian, T.H. Feng, D.S. Chuu, J. Phys. 38 (2005) 2432.
[10] F.S. Chien, J.W. Chang, S.W. Lin, Y.C. Chou, T.T. Chen, S. Gwo, T.S. Chao, W.F. Hsieh, Appl. Phys. Lett. 76 (2000) 360.
[11] X.N. Xie, H.J. Chung, H. Xu, C.H. Sow, A.T. Wee, Appl. Phys. Lett. 84 (2004) 4914.
[12] X.N. Xie, H.J. Chung, H. Xu, C.H. Sow, A.T. Wee, J. Am. Chem. Soc. 126 (2004) 7665.
[13] S.F. Lyuksyutov, R.A. Vaia, P.B. Paramonov, S. Juhl, L. Waterhouse, R.M. Ralich, G. Sigalov, E. Sancaktar, Nat. Mater. 2 (2003) 468.
[14] B. Bhushan, X.D. Li, J. Mater. Res. 12 (1997) 54.
[15] K.A. Ratter, J.W. Lyding, Nanotechnology 19 (2008) 15704.
[16] W.A. Ducker, T.J. Senden, R.M. Pashley, Nature 353 (1991) 239.
[17] C. Neto, V.S.J. Craig, Langmuir 17 (2001) 2097.
[18] S.R. Jian, T.H. Fang, D.S. Chuu, J. Phys. D: Appl. Phys. 38 (2005) 2432.
[19] Y.H. Liu, T. Wu, D.F. Evans, Langmuir 10 (1994) 2241.
[20] B. Bhushan, Handbook of Micro/Nano Tribology, second ed., CRC Press, Boca Raton, FL, 1994.
[21] T. Teuschler, K. Mahr, S. Miyazaki, M. Hundhausen, L. Ley, Appl. Phys. Lett. 67 (1995) 3144.
[22] P. Avouris, T. Hertel, R. Martel, Appl. Phys. Lett. 71 (1997) 285.
[23] J. Cervenka, R. Kalousek, M. Bartosik, D. Skoda, O. Tomanec, T. Sikola, Appl. Surf. Sci. 253 (2006) 2373.
[24] B. Marchon, S. Vierk, N. Heiman, R. Fisher, M. Khan, Tribology and Mechanics of Magnetic Storage Systems, vol. VI, STLE Special publication SP-26, Park Ridge, IL, 1985, p. 16.
[25] G. Jing, B. Marchon, J. Appl. Phys. 78 (1995) 4206.
[26] V.V. Tsukruk, V.N. Bliznyuk, Langmuir 14 (1998) 446.